Research Article GU J Sci 38(3): 1346-1357 (2025) DOI: 10.35378/gujs.1609655

Gazi University

Journal of Science

http://dergipark.org.tr/gujs

Experimental Investigation of Circumferential Temperature Variation in Large-Diameter Wickless Glass Heat Pipes

Ahmet OZSOY[1, *], Ayse KAYACAN[2]

[1]Isparta University of Applied Sciences, Department of Mechanical Engineering, 32200, Isparta, Türkiye
[2]Isparta University of Applied Sciences, Graduate Education Institute, 32200, Isparta, Türkiye

Highlights

- Circumferential temperature difference increases with heat load, peaking at 48°C under 100 W.
- Thermal resistance is min. at 30°, max. at 90°, influenced by circumferential temperature changes.
- At 90°, poor wetting causes local overheating, altering circumferential temperature distribution.
- Circumferential temperature variations impact heat transfer efficiency in wickless glass heat pipes.

Article Info

Received: 30 Dec 2024
Accepted: 18 Mar 2025

Keywords

Glass heat pipe
Thermosyphon
Wickless heat pipe
Thermal resistance

Abstract

This study investigates the circumferential temperature distribution in large-diameter wickless glass heat pipes under different inclination angles and heat loads. The experimental analysis was carried out on borosilicate glass heat pipes using ethanol as the working fluid. Surface temperatures were recorded at several axial and circumferential positions under heat loads ranging from 25 W to 100 W and inclination angles of 30°, 60°, and 90°. The results showed that heat transfer efficiency and thermal resistance varied significantly with inclination angle. The system showed optimum performance with lower thermal resistance and higher heat transfer efficiency at 30° and 60° inclination angles. However, increased surface temperatures and dry-out zones at 90° inclination negatively affected the heat transfer efficiency. The results highlight the importance of the use of wicks in the design of glass heat pipes for solar energy applications.

1. INTRODUCTION

Efficient heat transfer between media is crucial, but the energy consumption during this process is an even more critical factor. Among the various heat transfer devices, heat pipes are distinguished by their ability to function without external energy. The first example of such a system was the Perkins tube. The fundamental principles of heat pipes were first established by Gaugler in 1944 and Trefethen in 1962, and were subsequently named “Heat Pipe” by Grover in 1964 [1]. Heat pipes can be produced in various sizes and shapes across a broad temperature range. As passive heat transfer devices, they are employed in numerous fields, including electronic cooling, nuclear power plants, HVAC systems, heat recovery, and solar energy systems [1-3].

In recent years, vacuum tube solar energy systems have gained popularity. In such systems, the vacuum surrounding the glass tube minimizes heat losses, while the selective surface coating reduces radiative heat transfer. These systems demonstrate greater efficiency than flat-plate collectors. Vacuum tube systems can be classified into three principal categories. The aforementioned categories of vacuum tube systems include U-pipe systems and heat pipe systems.

Glass heat pipes are used in all-glass heat pipe solar collectors and are less common than vacuum tube copper heat pipe solar collectors. The thermal conductivity of glass is significantly lower than that of metals (e.g., copper or aluminum), with approximately only 1% of the thermal conductivity of copper. However, glass exhibits superior corrosion resistance compared to metals, as copper and aluminum do not possess the same level of corrosion resistance. In vacuum tube copper heat pipe solar energy systems, the energy

*Corresponding author, e-mail: ahmetozsoyr@isparta.edu.tr

received from the sun is transferred from the glass to the internal environment (air), from which it is then transferred to the heat pipe with fins. The heat pipe subsequently facilitates the transfer of this energy to water through phase transformation. In contrast, in all-glass heat pipe systems, the energy received from the sun is directly transferred to the water through phase transformation. Both types of heat pipes are gravity-assisted, and no wick is used in the pipe. The diameter of the glass heat pipe is approximately four times larger than that of the copper heat pipe; however, the amount of working fluid in glass heat pipes is lower than in copper heat pipe systems.

Early patents in this field were obtained by Fehliner and Ortabasi [4] and McConnel and Vansant [5]. Yin et al. [6] defined the working fluid properties and the optimal volume fraction for heat pipes. It has been reported that an all-glass heat pipe-based vacuum solar collector using ethyl alcohol as a working fluid achieves optimal heat recovery performance when the volume fraction of fluid is 1%. For water, the recommended volume fraction ranges between 0.08% and 1%. Fiaschi and Manfrida [7] investigated the compressive strength of glass tubes, confirming their durability at high temperatures. Their study indicated that an all-glass heat pipe solar collector with a 47 mm diameter and 1.5 mm thickness could withstand an internal pressure of 700 kPa at 150 °C, significantly lower than the 11000 kPa material strength.

In a study by Ribot and McConel [8], micrometer-sized glass beads adhered to the glass surface with sodium silicate solution to create a porous wick structure. The glass tube was annealed at 300 °C for three hours to ensure adhesion. Methanol was used as the working fluid, with 25% more than the amount needed to saturate the wick. Test results showed that the efficiency of the modified system was comparable to that of a full glass heat pipe, with the efficiencies of both systems being very close to each other.

A reflective film was applied to the bottom of the outer tube to enhance energy transport in an all-glass heat pipe vacuum tube solar collector [9]. The addition of the reflective film resulted in a 0.17% increase in optical efficiency, and an energy output of 87 W was achieved under quasi-thermal equilibrium conditions. The study also determined that the maximum temperature recorded by a thermal camera on the heat pipe was 96.1 °C. Furthermore, an analysis of the maximum thermal stress at the junction between the glass heat pipe and the vacuum tube revealed that the expected thermal stress was well below the material limits. This finding suggests that thermal stress is unlikely to pose a problem for the glass heat pipe vacuum tube.

Özsoy and Çimen [10] examined the impact of fluid charge volume on the performance of a glass heat pipe solar collector. They tested heat pipes filled with 3 ml and 4 ml of ethanol, finding that the 4 ml system exhibited a 3%-15% efficiency increase. Another study [11] investigated the effect of binary fluid mixtures on efficiency, evaluating combinations such as 75% ethanol - 25% water, 50% ethanol - 50% water, and 50% methanol - 50% water. The 75% ethanol - 25% water mixture provided the highest efficiency at 83%. Çimen et al. [12] reported a 77.5% efficiency at 85 °C by reducing the working fluid volume, thus preventing thermosyphon solar collector overheating.

This study is based on the research by Özsoy and Kolay [13], who conducted an experimental investigation of the surface temperature distribution and total thermal resistance in a 37 mm diameter, 1850 mm long glass heat pipe. They used 3 ml of ethanol and measured evaporator surface temperatures at seven points along the pipe, with one point dedicated to circumferential temperature distribution. The tests covered power levels from 30 W to 120 W at inclination angles of 30°, 45°, and 60°. Initially, the surface temperature increased rapidly before stabilizing. At 120 W power, a 70 °C temperature difference was observed between the top and bottom of the heat pipe. Thermal resistance analysis indicated that while a 30° inclination was advantageous, thermal resistances at steady-state conditions were similar across all angles. Furthermore, circumferential temperature measurements showed that the temperature difference increased with applied heat load.

Zhang et al. [14] examined the impact of integrating an all-glass heat pipe into parabolic trough systems. They analyzed thermal power and resistance variations at inclination angles from 10° to 80°. At 30°, the maximum thermal power recorded was 237 W, while at 80°, it dropped to 147 W. Thermal resistances decreased significantly from 10° to 50° before increasing rapidly after 60°. The lowest thermal resistance,

0.37 K/W, was observed at 50° inclination with a 230 W heat input. However, circumferential temperature distribution was not analyzed.

A numerical study by Chen et al. [15] investigated fluid selection for large-diameter and very-long heat pipes for extracting heat from underground hot dry rock formations. The study examined pressure drop and temperature gradient variations for different working fluids in heat pipes with diameters from 100 mm to 500 mm and lengths up to 4000 m. However, circumferential temperature distribution was not addressed.

Zhang et al. [16] stated that the surface tension effect decreases in large-diameter heat pipes, and a different flow regime emerges in these pipes. In a separate study, a large, separated low-heat-flux heat pipe for cooling a spent fuel pool was modeled [17-19], with evaporator and condenser tube diameters ranging from 65 mm to 100 mm. Due to the substantial diameter and minimal wall heat flux, the flow patterns in the evaporator deviate from those observed in conventional pipes.

The conventional heat pipe vacuum tube solar collector was tested by Said et al. [20], and the temperatures of the top and bottom surfaces of the vacuum tube were measured. At an irradiance of 1000 W/m², the temperature of the top surface of the vacuum tube was recorded as 145 °C, while the bottom surface registered a temperature of 62 °C. At irradiation intensities of 1000 W/m², 500 W/m², and 300 W/m², the temperature differences between the upper and lower surfaces were measured as 83 °C, 79 °C, and 69 °C, respectively. It is evident that an increase in irradiation intensity leads to an increase in surface temperatures.

Existing studies have mostly focused on small-diameter metal heat pipes [21-25]. In current studies, heat pipes typically possess relatively small diameters and are composed of metal materials. The high thermal conductivity of these metal materials results in a modest circumferential temperature difference. This may explain why the peripheral temperature distribution has not been thoroughly examined. In contrast, glass heat pipes are fabricated with a larger diameter and lack a wick. The glass material used results in a relatively smooth surface. The wettability of the glass surface by the working fluid is low, and this, combined with the low thermal conductivity of glass, is expected to negatively affect the performance of the heat pipe. The circumferential temperature distribution is particularly important in glass heat pipes due to their larger diameter, low thermal conductivity, and small amount of working fluid.

This study aims to experimentally determine irregularities in circumferential temperature distribution in large-diameter wickless glass heat pipes to address this research gap.

2. MATERIALS AND METHODS

The heat pipes used in this study were made of borosilicate glass and operated based on gravity assistance, as they lacked a wick structure. The working fluid was ethanol. The internal diameter of the glass heat pipes was 33.8 mm, while the external diameter was 37.0 mm. The evaporator length was 1400 mm, the condenser length 125 mm, and the adiabatic length 125 mm, giving a total length of 1650 mm. The glass heat pipes were evacuated to 4×10^{-3} Pa and charged with 4 ml of ethanol before being sealed to maintain the vacuum.

Surface temperature measurements were conducted at five different locations along the evaporator section and at one location in the adiabatic section. At each location, temperature data were collected from four circumferential points positioned at 90° intervals. Since the condenser section was enclosed within a jacket, direct surface temperature measurements were not feasible. Instead, K-type thermocouples were used, while the inlet and outlet water temperatures in the condenser jacket were recorded using PT100 sensors. As depicted in Figure 1, temperature measurements were taken at multiple points along the heat pipe. Figure 2 illustrates the placement of thermocouples.

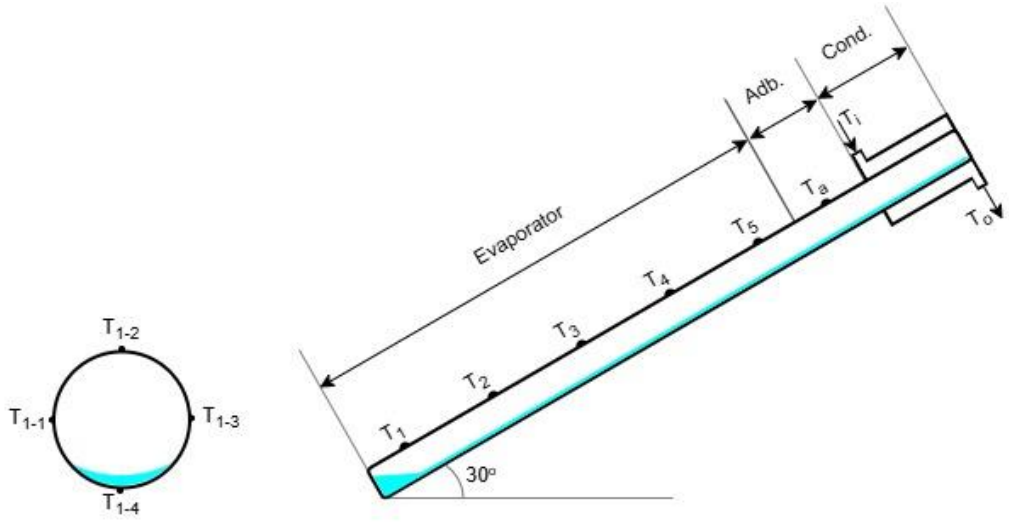

Figure 1. *Temperature measurement points on the glass heat pipe*

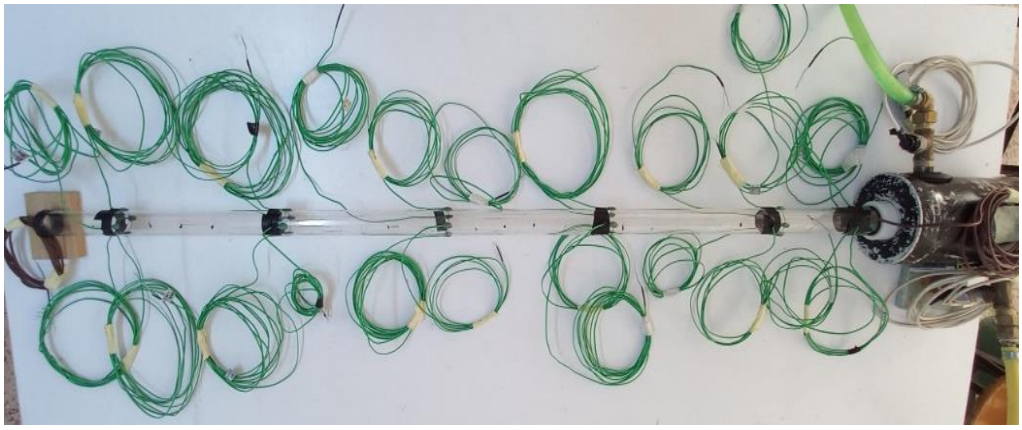

Figure 2. *View of thermocouples on the glass heat pipe*

As shown in Figure 1, the temperature distribution along the evaporator surface (axial) is represented by T_1 to T_5, while T_a represents the surface temperature of the adiabatic section. Additionally, the circumferential temperature distribution of the heat pipe was measured at four points for each location (e.g., T_{1-1}, T_{1-2}, T_{1-3}, T_{1-4} for point 1). The temperatures of the water entering and exiting the cooling jacket in the condenser were recorded as T_i and T_o, respectively.

The characteristics of the heat pipes are outlined in Table 1, while the experimental study parameters are enumerated in Table 2.

Table 1. *Properties of the glass heat pipes*

Heat pipe material	Borosilicate-33
Outer diameter (mm)	37.0
Inner diameter (mm)	33.8
Evaporator section length (mm)	1340
Adiabatic section length (mm)	125
Condenser section length (mm)	125
Working fluid quantity (mL)	4
Working fluid	Ethanol
Internal pressure (Vacuum) (Pa)	$4x10^{-3}$

Table 2. *Experimental study parameters*

Evaporator section heat load (W)	25, 50, 75, 100
Heat pipe inclination angle (°)	30, 60, 90
Condenser jacket fluid flow rate (l/min)	0.18

The desired heat load was applied via an electrical connection to a variac-controlled resistance wire wound around the evaporator section. A wattmeter was used to measure electrical power input. To minimize heat loss to the surroundings, the heat pipe was insulated with 20 mm of glass wool, while the condenser section was insulated with 15 mm of polyurethane. Heat was removed from the condenser section via water cooling, with flow rates carefully controlled. Figure 3 presents a photograph of the experimental setup.

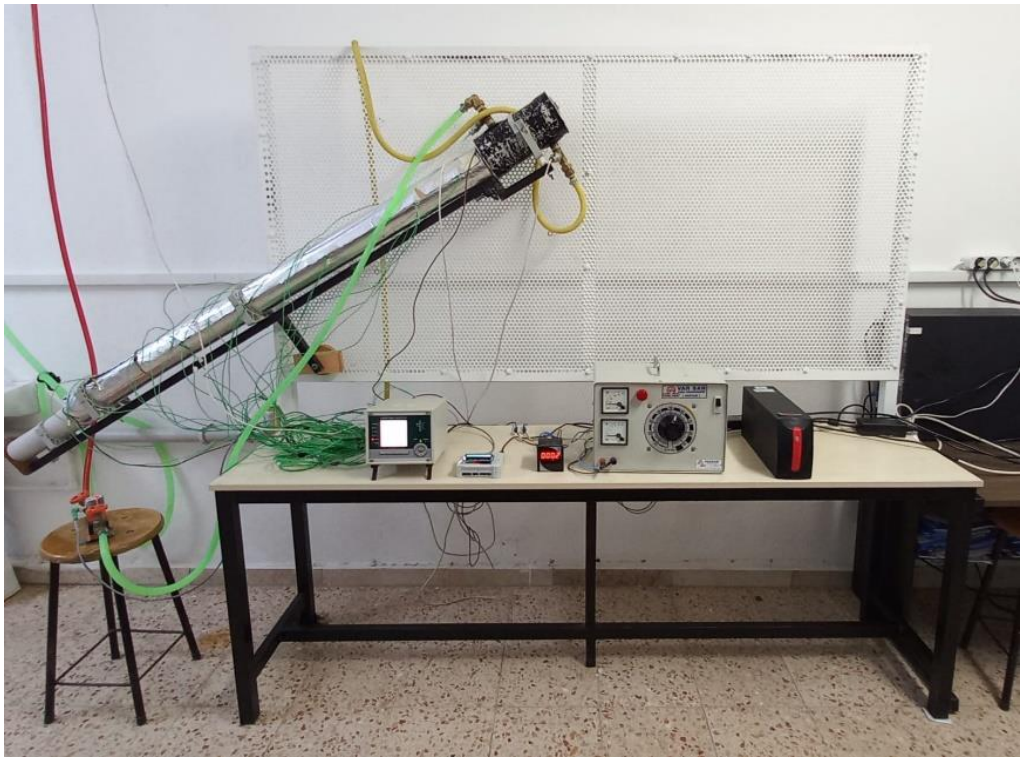

Figure 3. *View of the experimental setup*

In the experimental study, the heat load (Q_i) applied from the evaporator section was determined by measuring the current (I) and voltage (V) of the spirally wound resistance wire (Equation (1))

$$Q_i = V\ I\ . \tag{1}$$

In order to determine the surface temperatures in the evaporator section of the heat pipe, measurements were taken at five distinct locations, as well as one additional point in the adiabatic section. At each measuring point, four circumferential temperatures were recorded at 90° intervals. Surface temperature measurements were made using K-type thermocouples, and the average temperature for each point on the heat pipe surface was calculated as the average of the four circumferential temperature values. For example, the average temperature at point 1 of the evaporator section (T_1) was calculated as follows (Equation (2)):

$$T_1 = \frac{T_{1-1}+T_{1-2}+T_{1-3}+T_{1-4}}{4}. \tag{2}$$

The average temperature of the evaporator section (T_e) is also the average of the surface temperatures (Equation (3)).

$$T_e = \frac{T_1+T_2+T_3+T_4+T_5}{5}. \tag{3}$$

The circumferential temperature difference for each measurement point is calculated as follows, using the example of point 1 (Equation (4)):

$$\Delta T_1 = T_{1-2} - T_{1-4} \,. \tag{4}$$

The heat extracted from the condenser area was facilitated through the use of a body-tube-type heat exchanger, and the fluid flow rate was determined using an ultrasonic flow meter. The thermal power ($\dot{Q}_c$) from the condenser section is calculated by Equation (5)

$$\dot{Q}_c = \dot{m}\, C_p\, (T_o - T_i) \,. \tag{5}$$

In this context, T_i and T_o represent the inlet and outlet temperatures of the fluid entering the condenser section, C_p refers to the specific heat of water, and $\dot{m}$ represents the mass flow rate.

The ratio of the difference between the surface temperatures of the evaporator and condenser sections to the heat load determines the thermal resistance (R_e) of the heat pipe (Equation (6)).

$$R_e = \frac{(T_e - T_a)}{Q_i}. \tag{6}$$

In this context, T_e represents the average surface temperature of the evaporator section, T_a denotes the temperature of the adiabatic section surface and Q_i signifies the power applied to the heat pipe from the evaporator section.

3. FINDINGS AND DISCUSSION

The effect of varying heat loads and inclination angles on the circumferential temperature distribution was analyzed. Figures 4, 5, 6, and 7 illustrate temperature variations at different conditions. Heat applied to the evaporator section was carried through phase transformation of the working fluid.

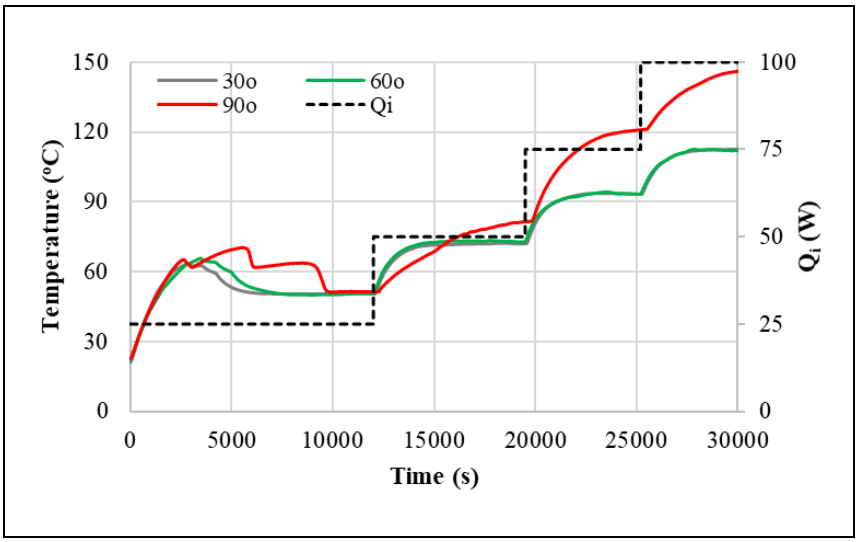

Figure 4. *Variation of average evaporator section temperature with different inclination angles*

Figure 4 demonstrates the average evaporator temperature change over time. As the heat load increased from 25 W to 100 W, the average evaporator temperature rose. At 30° and 60° inclinations, the temperatures remained similar, whereas at 90°, the temperatures were significantly higher. The average temperature at 100 W was 112 °C for 30° and 60°, but increased to 146 °C at 90°. During the operation of the heat pipe at inclination angles of 30° and 60°, the liquid working fluid returning from the condenser to the evaporator, under the effect of gravity, always flows from the bottom side of the heat pipe (in the regions where the thermocouples $T_{5\text{-}4}$, $T_{4\text{-}4}$, $T_{3\text{-}4}$, $T_{2\text{-}4}$, and $T_{1\text{-}4}$ are mounted). At an inclination of 90°, it is postulated that the

return of the fluid from the condenser to the evaporator occurs from different circumferential locations. Furthermore, the fluid droplet may return rapidly from the condenser surface to the evaporator without sufficiently wetting or only partially wetting the surface. It can be surmised that the temperature increases and the evaporator section experiences desiccation due to insufficient wetting of the surfaces at a 90° inclination. Additionally, the relatively large diameter of the heat pipe reduces the surface tension effect of the fluid, thereby preventing the working fluid from adequately wetting the inner surface of the heat pipe [13]. For different inclination angles, the time required for the glass heat pipes to start operating and reach a steady state is 5900 s at a 30° inclination, 7600 s at 60°, and 10,000 s at 90°. As the inclination angle increases from horizontal to vertical, the contact area between the working fluid and the evaporator surface decreases, leading to a reduction in film evaporation on the surface.

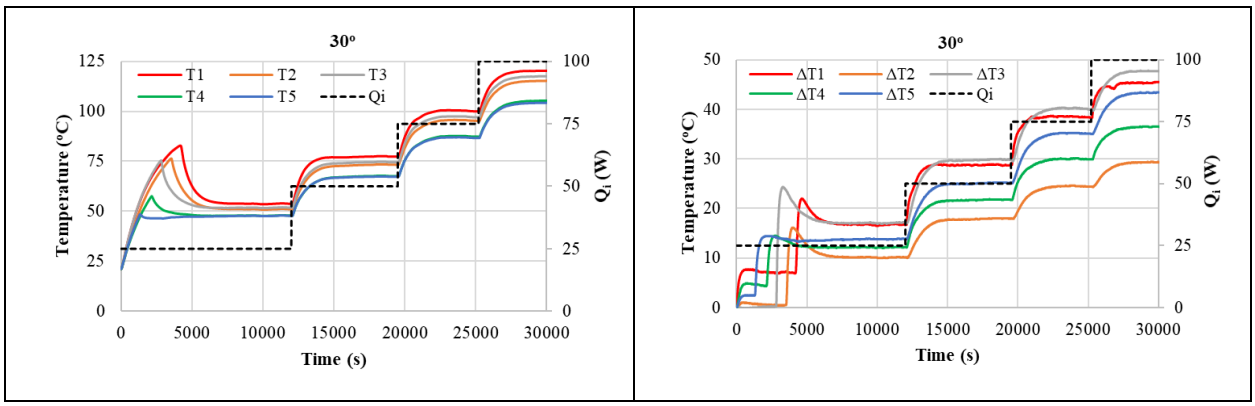

Figure 5. *Average circumferential temperatures (left) and variation in temperature difference (right) for the evaporator section of the heat pipe at a 30° inclination angle*

Figure 5 presents the average temperatures recorded at points 1, 2, 3, 4, and 5, as well as the circumferential temperature difference, during the operation of the heat pipe at a 30° inclination angle under varying heat loads. When a 25 W heat load was initially applied to the heat pipe, it was observed that point 5, which is closest to the condenser region, reached a steady-state temperature first. Subsequently, the temperatures at the other points stabilized gradually in accordance with their distance from the condenser. As the thermal power applied to the evaporator section increased, the average temperature also rose. Under a 25 W heat load, the temperatures across the entire surface of the heat pipe reached a steady state in approximately two hours. The extended time required for stabilization is attributed to the low thermal conductivity of the glass material.

Additionally, due to the limited amount of working fluid, phase change within the heat pipe predominantly occurs through film evaporation of the returning liquid from the condenser to the evaporator, rather than through pool boiling, which further prolongs the stabilization period. As the thermal power applied to the evaporator section increases, surface temperatures initially rise and subsequently decrease before reaching a steady state. Moreover, it is evident that the temperature difference between the average surface temperatures measured along the evaporator section increases with the applied thermal power.

For each measurement point, temperature differences are defined as the variations observed between the values recorded at the top and bottom surface points (see Figure 1). For instance, ΔT_1 represents the temperature difference between $T_{1\text{-}2}$ and $T_{1\text{-}4}$ at point 1, and similarly, ΔT_2 denotes the temperature difference between $T_{1\text{-}2}$ and $T_{1\text{-}4}$ at point 2. As demonstrated in Figure 5, the temperature difference increases in proportion to the applied electrical power in the evaporator section. The measured temperature difference ranged from 10 °C to 17 °C under a 25 W heat load, whereas it varied between 29 °C and 48 °C under a 100 W heat load.

Although the resistance wire used to supply heat to the evaporator section was spirally wound along the entire pipe, it is still possible that the thermocouples were partially affected by the heating wires despite the precautions taken.

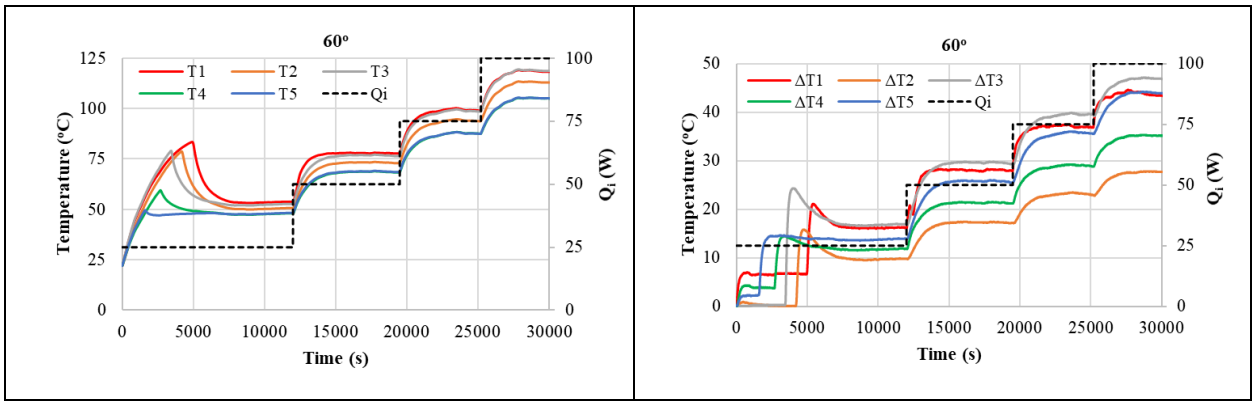

Figure 6. *Average circumferential temperatures (left) and variation in temperature difference (right) for the evaporator section of the heat pipe at a 60° inclination angle*

Figure 6 shows the average temperatures at the measurement points of the heat pipe operated at a 60° inclination angle and subjected to different heat loads, as well as the temperature difference between the top and bottom points. As shown in the figure, the overall trend is similar to that observed when the heat pipe was operated at a 30° inclination. When thermal power was applied to the evaporator section at 25 W, 50 W, 75 W, and 100 W, the corresponding average temperatures were measured to be 50 °C, 70 °C, 100°C, and 115 °C, respectively. While the temperature difference between the measurement points varied with the applied thermal load, the lowest temperature difference was recorded as 10 °C at 25 W, and the highest temperature difference was 47 °C at 100 W.

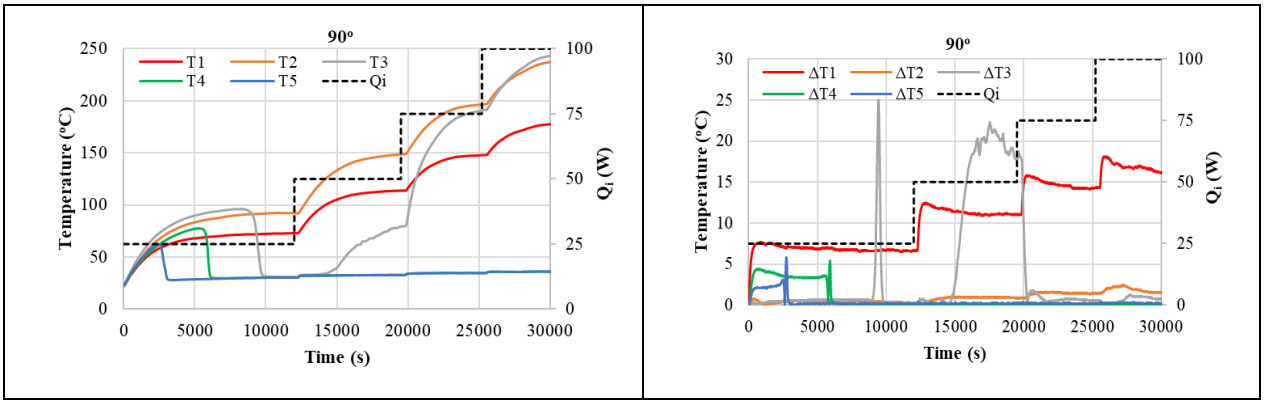

Figure 7. *Average circumferential temperatures (left) and variation in temperature difference (right) for the evaporator section of the heat pipe at a 90° inclination angle*

Figure 7 illustrates the average temperatures and the upper-lower temperature differences at the measurement points of the heat pipe operating at a 90° inclination angle under varying heat loads. The results obtained at a 90° inclination angle differ from those recorded at 30° and 60° inclination angles. When thermal power application began at 25 W, the temperatures at all measurement points increased similarly. At approximately 2500 s, when the liquid-phase fluid returning from the condenser region reached point 5, film evaporation occurred, leading to a decrease in surface temperature. A similar phenomenon was observed at point 4 at 5700 s and at point 3 at 8600 s. As shown in the figure, no temperature decrease was observed at points 1 and 2, indicating that the fluid did not reach these regions, resulting in local dry-out.

When the thermal power was increased to 50 W, film evaporation was observed only in the regions where points 4 and 5 were located, while the other regions remained dry due to the absence of fluid, leading to an increase in surface temperatures. At 100 W, the surface temperatures at points 1, 2, and 3 ranged between 177 °C and 243 °C. The primary cause of these elevated temperatures is attributed to local dry-out, which occurs when the surface is not wetted by saturated liquid.

When the heat pipe operates at 30° and 60° inclination angles, the liquid returning from the condenser to the evaporator under gravitational influence consistently flows along the bottom surface of the pipe, wetting the areas it passes through. However, the temperature differences shown in Figure 7 exhibit a distinct pattern compared to those at 30° and 60° inclination angles. The most significant temperature difference was recorded as 18 °C at point 1 under 100 W thermal power. At points 3 and 4, the temperature differences fluctuate over time but remain relatively insignificant.

The primary reason for the different temperature variations at a 90° inclination is that the returning fluid moves directly downward due to gravity, eliminating the distinct bottom surface characteristic present at lower inclination angles. Instead, the fluid is likely to flow along the entire circumferential surface, which contributes to the lower observed temperature differences. However, a low-temperature difference at a given point does not necessarily indicate a lower temperature in that region. For instance, at 100 W thermal power, the circumferential temperature at point 2 was measured at 242 °C, yet the temperature difference was only 2 °C.

It is hypothesized that the temperature peaks observed at point 3, occurring between 10000 seconds and 15000–20000 seconds, result from changes in the direction of liquid flow. As the liquid travels along the inner surface of the vertically oriented (90°) heat pipe, from the condenser to the evaporator under the influence of gravity, variations in the flow direction likely cause temperature fluctuations, leading to the observed peaks.

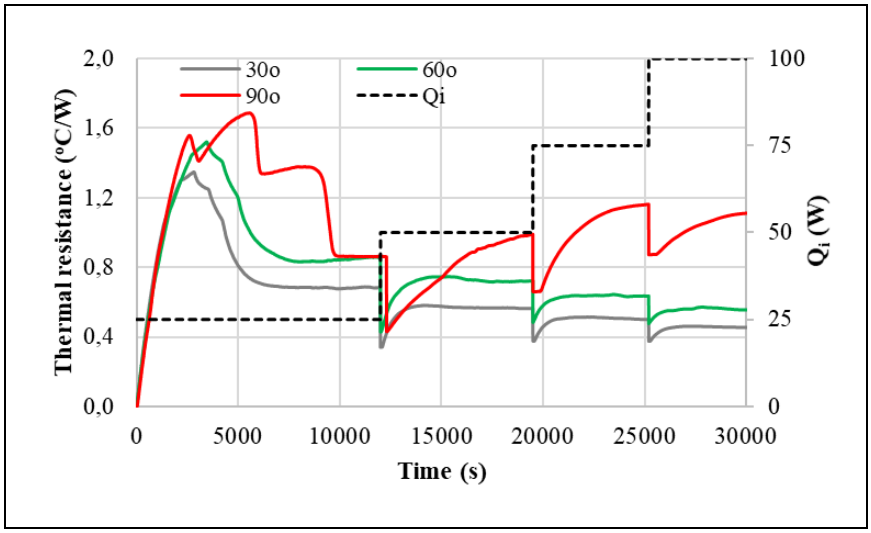

Figure 8. *Variation of evaporator section thermal resistance with inclination angle*

Figure 8 illustrates the variation in thermal resistance values for the evaporator section. As the power applied to the evaporator section increases, thermal resistance decreases. This result holds for the normal operation (30° and 60° inclination) of the heat pipe; however, a partial increase in thermal resistance is observed with an increase in thermal power at a 90° inclination angle. The reason for this is explained by the high temperatures observed at specific points in the evaporator region, as shown in more detail in Figure 7, and by the average evaporator temperature graph presented in Figure 4. As illustrated by the presented data, specific regions of the heat pipe (designated as points 1, 2, and 3) are found to be non-functional due to a process of dry-out. This phenomenon signifies the inability of these regions to be adequately wetted by the working fluid, consequently leading to elevated temperatures. The rise in temperature, in turn, results in an escalation in thermal resistance.

When comparing inclination angles, the lowest thermal resistance occurs at a 30° angle, while the highest thermal resistance is observed at a 90° angle. The lowest thermal resistance, which corresponds to the lowest average surface temperature, is obtained at the 30° inclination angle. In contrast, the highest thermal resistance, associated with the highest average surface temperature, is observed at the 90° inclination angle. Consequently, since there is little change in the condenser surface temperature, the variable that

predominantly determines the change in thermal resistance is the evaporator region temperature. As the evaporator region temperature increases, thermal resistance also increases. The results of Zhang et al. [15] also indicate that as solar radiation reaching the surface of the glass heat pipe increases from 600 W/m² to 1100 W/m², a decrease in thermal resistance is observed.

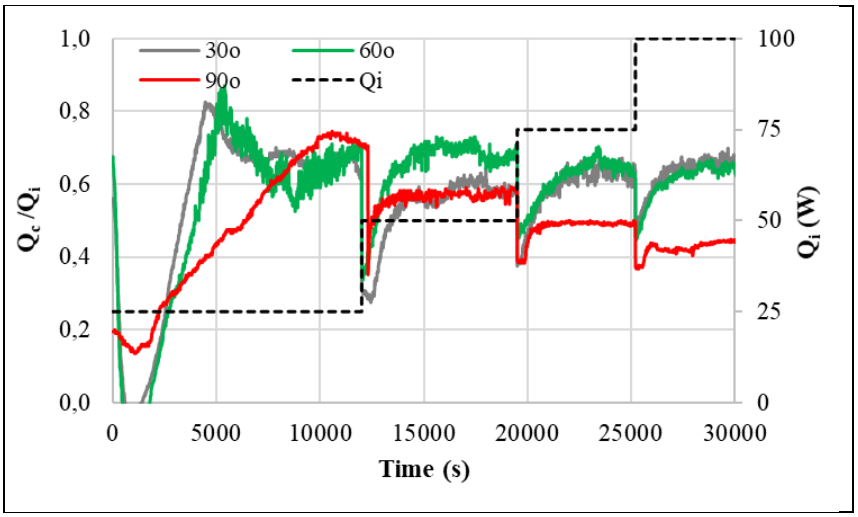

Figure 9. *Variation of heat pipe efficiency with inclination angle*

As demonstrated in Figure 9, the ratio of power applied to the evaporator section of the heat pipe to the heat transferred from the condenser section varies. The figure reveals that the efficiency at 30° and 60° inclination angles is comparable. However, at a 90° inclination angle, the efficiency is typically lower than at the other two angles. The elevated temperatures observed on the evaporator surface of the heat pipe can be attributed to the inhibition of heat transfer, resulting from the inability to wet the inner surfaces. This phenomenon indicates insufficient heat transfer from the surface to the working fluid in regions where the temperature is elevated, leading to a decrease in efficiency. The efficiency at 30° and 60° is approximately 65%, whereas at a 90° inclination angle, the efficiency drops to as low as 40%. This decline in efficiency at 90° can be attributed to the increase in thermal resistance caused by the high temperature, which results from the incomplete wetting of the evaporator surface, leading to dry-out in certain areas.

4. CONCLUSION

This study experimentally investigated the circumferential temperature variation in large-diameter wickless glass heat pipes. The results demonstrated that:

- Heat transfer efficiency is significantly influenced by the inclination angle, with optimal performance observed at 30° and 60°. At 90°, heat transfer is hindered by high surface temperatures and dry-out regions, which reduce efficiency.
- Thermal resistance is lowest at 30° due to better fluid distribution, while it increases at 90° due to poor wetting of the inner surfaces, leading to dry-out and higher temperatures in certain regions.
- The circumferential temperature variation along the heat pipe is not homogeneous. While the peripheral temperature difference is similar at 30° and 60° inclinations, it is much larger at 90°, particularly toward the lower of the heat pipe, where dry-out occurs.
- At 30° and 60° inclinations, the upper part of the heat pipe consistently reaches the highest temperatures, while the lower part remains cooler due to more effective wetting of the surface by the working fluid.
- High surface temperatures result in increased thermal resistance, which contributes to a decrease in efficiency. This effect is particularly pronounced at 90°, where incomplete wetting leads to elevated temperatures and reduced heat transfer.

The findings under consideration emphasize the significance of inclination angle and fluid behavior in optimizing the performance of wickless glass heat pipes for solar energy applications. In order to enhance performance and reduce the circumferential temperature distribution, it is imperative to increase the wetting

of the entire evaporator surface. This objective can be accomplished by incorporating a wick into the heat pipe.

ACKNOWLEDGMENT

We would like to express our gratitude to Mert Çimen and Sistem Enerji (Nazilli/Aydın) for their assistance in the custom production of the glass heat pipes, which were utilized in this study.

CONFLICTS OF INTEREST

No conflict of interest was declared by the authors.

REFERENCES

[1] Faghri, A., Heat Pipe Science and Technology, Taylor and Francis, London, (1995).

[2] Reay, D., Kew, P., McGlen, R., Heat Pipes-Theory, design and applications, Sixth edition, Elsevier, Oxford, (2014).

[3] Zohuri, B. Heat Pipe Design and Technology. Modern Applications for Practical Thermal Management, Second Edition, Springer, (2016).

[4] Fehliner, F.P., and Ortabasi, U., "Solar heat pipe", U.S. Patent, Patent Number: 4.067.315, (1978).

[5] McConnell, R.D., and Vansant J.H., "Glass heat pipe evacuated tube solar collector", U.S. Patent, Patent Number: 4.474.170, (1984).

[6] Yin, Z., Yan, X., Niu, C., and Li, V., "Glass vacuum heat pipe type solar heat collection pipe", European Patent, Patent Number: 1.752.720.B1, (2017).

[7] Fiaschi, D., and Manfrida G., "Model to predict design parameters and performance curves of vacuum glass heat pipe solar collectors", Energy, 58: 28-35, (2013). DOI: https://doi.org/10.1016/j.energy.2012.12.028

[8] Ribot, J., and McConnell, R.D., "Testing and analysis of a heat-pipe solar collector", Journal of Solar Energy Engineering, 105: 440-445, (1983). DOI: https://doi.org/10.1115/1.3266405

[9] Gong, J., Sun, Z., Wang, J., and Lund, P.D., "Performance studies of novel all-glass heat pipe evacuated collector tube integrating numerical simulation and experiment method", Solar Energy, 253: 491-500, (2023). DOI: https://doi.org/10.1016/j.solener.2023.02.028

[10] Özsoy, A., and Çimen, M., "Experimental investigation of the effect of fluid charge amount on the glass heat pipe solar collector efficiency", 22. Congress on Thermal Science and Technology, Kocaeli, 1: 546-550, (2019).

[11] Özsoy, A., and Çimen, M., "Experimental investigation of the use of binary mixtures as a work fluid in vacuum tube glass heat pipe solar collectors", 22. Congress on Thermal Science and Technology, Kocaeli, 1: 541-545, (2019).

[12] Çimen, M., Colakoglu, M., and Güngör, A., "Overheating limitation of thermosiphon solar collectors by controlling heat pipe fluid in all glass evacuated tubes", Solar Energy, 230: 515-527, (2021). DOI: https://doi.org/10.1016/j.solener.2021.10.066

[13] Özsoy, A., and Kolay, P., "Experimental investigation of surface temperature and thermal resistance of all glass heat pipe under different operating conditions", 23. Congress on Thermal Science and Technology, Kocaeli, 1: 659-666, (2021).

[14] Zhang, C., Zhang, X., Zhu, J., and Chen, F., "Non-imaging concentrator coupled with all-glass solar superconducting heat pipe and its photothermal conversion characterization studies", Energy Conversion and Management, 325: 119367, (2025). DOI: https://doi.org/10.1016/j.enconman.2024.119367

[15] Chen, J., Huang, W., Cen, J., Cao, W., Li, Z., Li, F., and Jiang, F., "Heat extraction from hot dry rock by super-long gravity heat pipe: Selection of working fluid", Energy, 255: 124531, (2022). DOI: https://doi.org/10.1016/j.energy.2022.124531.

[16] Zhang, P., Wang, B., Shi, W., and Li, X., "Experimental investigation on two-phase thermosyphon loop with partially liquid-filled downcomer", Applied Energy, 160: 10-17, (2015). DOI: https://doi.org/10.1016/j.apenergy.2015.09.033

[17] Ye, C., Zheng, M.G., Wang, M.L., Zhang, R.H., and Xiong, Z.Q., "The design and simulation of a new spent fuel pool passive cooling system", Annals of Nuclear Energy, 58: 124-131, (2013). DOI: https://doi.org/10.1016/j.anucene.2013.03.007

[18] Kuang, Y.W., Wang, W., Zhuan, R., and Yi, C.C., "Simulation of boiling flow in evaporator of separate type heat pipe with low heat flux", Annals of Nuclear Energy, 75: 158-167, (2015). DOI: https://doi.org/10.1016/j.anucene.2014.08.008

[19] Kuang, Y.W, Yi, C.C., and Wang, W., "Modeling and simulation of large-scale separated heat pipe with low heat flux for spent fuel pool cooling", Applied Thermal Engineering, 147: 747-755, (2019). DOI: https://doi.org/10.1016/j.applthermaleng.2018.10.124

[20] Said, S., Mellouli, S., Alqahtani, T., Algarni, S., Ajjel, R., Ghachem, K., and Kolsi, L., "An Experimental Comparison of the Performance of Various Evacuated Tube Solar Collector Designs", Sustainability, 15(6): 5533, (2023). DOI: https://doi.org/10.3390/su15065533

[21] Mathew, A.A., and Thangavel, V., "A novel thermal energy storage integrated evacuated tube heat pipe solar dryer for agricultural products: Performance and economic evaluation", Renewable Energy, 179: 1674-1693, (2021). DOI: https://doi.org/10.1016/j.renene.2021.07.029.

[22] Bouadila, S., Rehman, T., Baig, M.A.A., Skouri, S., and Baddadi, S., "Energy, Exergy and Economic (3E) analysis of evacuated tube heat pipe solar collector to promote storage energy under North African climate", Sustainable Energy Technologies and Assessments, 55: 102959, (2023). DOI: https://doi.org/10.1016/j.seta.2022.102959.

[23] Nithyanandhan, K., Suganeswaran, K., and Murugan, P.C., "Experimental study on heat pipe evacuated tube solar collector for residential use with various condenser configurations", Energy Conversion and Management, 312: 118583, (2024). DOI: https://doi.org/10.1016/j.enconman.2024.118583.

[24] Alshukri, M.J., Hussein, A.K., Eidan, A.A., and Alsabery, A.I., "A review on applications and techniques of improving the performance of heat pipe-solar collector systems", Solar Energy, 236: 417-433, (2022). DOI: https://doi.org/10.1016/j.solener.2022.03.022.

[25] Henein, S.M., and Abdel-Rehim, A.A., "The performance response of a heat pipe evacuated tube solar collector using MgO/MWCNT hybrid nanofluid as a working fluid", Case Studies in Thermal Engineering, 33: 101957, (2022). DOI: https://doi.org/10.1016/j.csite.2022.101957.